Received March 27, 2020, accepted April 14, 2020, date of publication April 20, 2020, date of current version May 4, 2020.

Digital Object Identifier 10.1109/ACCESS.2020.2988666

A Novel NE-DFT Channel Estimation Scheme for Millimeter-Wave Massive MIMO Vehicular Communications

ZHAO YI[1], (Student Member, IEEE), AND WEIXIA ZOU[1,2], (Member, IEEE)
[1]Key Laboratory of Universal Wireless Communications, MOE, Beijing University of Posts and Telecommunications, Beijing 100876, China
[2]State Key Laboratory of Millimeter Waves, Southeast University, Nanjing 210096, China

Corresponding author: Weixia Zou (zwx0218@bupt.edu.cn)

This work was supported in part by the NSFC under Grant 61971063.

ABSTRACT Having the ability to provide an ultrafast and high-rate data exchange, millimeter-wave (mmWave) massive MIMO has been viewed as one of the technologies with the most potential for vehicular cellular systems in next-generation wireless communications. To alleviate the adverse influence of huge path losses, beamforming techniques are always introduced in various mmWave systems to provide sufficient channel gains. However, it is important to note that the traditional channel estimation algorithms may no longer be available in vehicular cellular networks due to the rapid movements of pedestrians and vehicles. Under this condition, this paper proposes a noise elimination-based discrete Fourier transform (DFT) channel estimation strategy, namely, the NE-DFT channel estimation strategy, for mmWave vehicular communications. Specifically, we first use the iterative cancellation method to initially estimate all path parameters. Then, to further improve the estimate accuracy, we set a decision threshold to determine the authenticity of the estimated paths. Furthermore, the energy distribution of each path in the channel is analyzed, and an additional estimation scheme is designed that enables a more accurate estimation of the previously estimated paths, which uses the comparison value between the total channel matrix energy and the actual signal matrix energy as an auxiliary judgment to successively select the path with the minimum comparison value until a sufficient number of real paths are selected. Finally, the channel matrix is reconstructed using the estimated channel parameters. Simulation results verify that the proposed NE-DFT channel estimation scheme can achieve much better NMSE performance than the conventional scheme, even in comparison with the time-variant channel.

INDEX TERMS Massive MIMO, millimeter-wave (mmWave), vehicular communication, channel estimation.

I. INTRODUCTION

Due to its wide bandwidth [1], [2] and high spectral efficiency [3]–[5], millimeter-wave (mmWave) massive multiple-input multiple-output (MIMO) has been considered as a key technique for 5th generation (5G) wireless communications to meet the significant growth of mobile traffic. Importantly, mmWave signals usually suffer from much high free-space path loss caused by high atmospheric attenuation [6], and even worse, these signals will suffer a greater path loss when they are blocked by obstacles such as buildings, foliage, and the user's body, etc. [7]. In addition, given the high maneuverability of the vehicle network, the beamforming needs to be completed in a short time, the channel coherence time between the base station (BS) and the mobile users (MS) is greatly reduced [8]–[10] and useful signals in the channel are susceptible to noise interference [11]–[14]. Fortunately, the benefit of the high directional power gain of beamforming can sufficiently compensate for the high path loss in the mmWave band, which guarantees a high signal-to-noise ratio (SNR) at the receiver to support extremely high data rate transmissions with large bandwidths [15], [16].

To date, numerous works have been conducted on the application of mmWave massive MIMO in various scenarios, i.e., cellular systems [1], [5] and vehicle to everything (V2X) communications [6], [9], [11], [12]. Taking the mmWave

The associate editor coordinating the review of this manuscript and approving it for publication was Chenhao Qi.

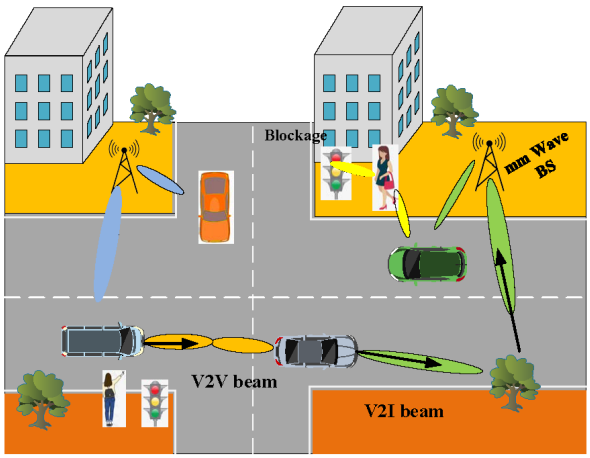

FIGURE 1. A mmWave V2X fast vehicle communication model.

massive MIMO V2X systems as an example, as shown in Fig.1, the BSs are built on the side of the road in the downtown area, the fast-moving vehicle users communicate with BS by mmWave within a short-range area, a vehicle directionally connects with other ones, roadside infrastructures, or pedestrians and vehicle to vehicle (V2V) and/or vehicle to infrastructure (V2I) communication links are simultaneously established. In this system, the beamforming process must be completed in an extremely short time given the adverse impact of fast-changing channel communication, and thus, timely and effective channel state information (CSI) is important to ensure the superiority of the mmWave massive MIMO scheme. Since the wireless conditions in vehicular networks are more severe than that in common cellular networks, higher demands are encountered on existing fast channel estimation techniques [6], [8], [9].

To address this issue, a number of research works focus on channel estimation of mmWave massive MIMO V2X communications in static or slowly time-variant cases [5], [11], [13], [17], [18]. In [7], [19], [20], the authors pointed out that mmWave massive MIMO communication is the only feasible way to achieve high-bandwidth connected vehicles. The authors in [12], [14] considered some key parameters affecting channel estimation accuracy, such as Doppler frequency, antenna patterns, etc. Moreover, the authors of [7] and [17] proposed to incorporate nested arrays into the analog array architecture in high-speed scenarios, and these schemes can effectively reduce the complexity and power consumption of the system. In addition, some works studied the channel estimation schemes in high-mobility vehicle cellular systems, such as the proposal of the authors in [6], in which a 3D structured orthogonal matching pursuit algorithm-based downlink channel estimation technique in high-mobility scenarios was reported that can achieve accurate CSI with low pilot overhead, and the work of [14] that transformed the channel estimation problem-based mmWave-OFDM system into a harmonic retrieval problem and proposed two methods to approximately acquire the maximum likelihood (ML) estimate. Unfortunately, existing schemes only considered the analog beamforming cases, which limited the processing capability of mmWave transceivers and caused a considerable performance loss, particularly for mobile users. Moreover, the deployment of an analog-only beamforming approach imposes several constraints on engineering and degrades the system performance. To overcome the limitations of analog beamforming and achieve good performance of digital beamforming, a new idea of hybrid beamforming is proposed in [1], [5], [7], which a multistage adaptive channel estimation algorithm is deployed to achieve spatial multiplexing gain by using multistream and multiuser transmission. In this regard, the authors in [21] and [22] proposed a feedback mechanism to adaptively adjust the length of the training sequence with the channel change to accurately estimate the channel. Unfortunately, the algorithms exhibit low estimation accuracy and requires a large number of feedback bits. Apart from that, the use of specific beam training and a new greedy channel estimator combination in the case of highly mobile users has been recently proposed [7], [19], [23], which can effectively estimate the sparse characteristics of the mmWave massive MIMO channel and the dynamic characteristics of the target user channel. Unfortunately, the algorithms need to perform the common beam training more frequently, which leads to higher training overhead. In [24] and [25], the power of each channel path is mainly concentrated on the intersection of two adjacent rows and two adjacent columns of the channel matrix, which is exploited to find the path with the maximum energy and the position of the main energy path is determined. Since the path energy is random distribute, it finds the path that maybe formed by side lobes or the peaks around the main lobe. However, our proposed algorithm can not only estimate the paths with the maximum energy, but also estimate more paths from channel that are seriously affected by noise. Especially, our proposed scheme can effectively estimate the useful signals that completely submerged by noise when users are moving fast.

Importantly, we note that the channel estimation schemes in the abovementioned works were studied under the assumption of static or slowly time-variant scenarios. However, in a fast changing channel scenario, such as in the mmWave massive MIMO vehicle system, those channel estimation algorithms may no longer be available due to the rapid movements of pedestrians and vehicles. However, to the best of the authors' knowledge, in a fast changing channel scenario, the existing schemes cannot adjust to the training sequence length with the channel changes, and a high-precision channel estimation algorithm has not been studied in the mmWave massive MIMO vehicle system, especially when the noise interference is severe.

To fill this gap, this paper proposes a novel noise elimination-based discrete Fourier transform (DFT) channel estimation scheme, called the NE-DFT channel estimation scheme, and analyzes the estimation performance. In the proposed channel estimation scheme, we first exploit

a conventional DFT-based channel estimation algorithm (DFT-CEA) to initially estimate all channel parameters [20]. To further improve the estimation accuracy, a threshold based on noise energy is proposed to judge the authenticity of the channel paths estimated by DFT-CEA. Furthermore, we analyze the energy distribution of channel paths and design an appropriate submatrix for energy extraction to estimate the paths whose energy is below a threshold, which can further eliminate noise interference. Finally, we perform a comparison calculation between the total channel matrix energy and the actual signal matrix energy to achieve a more accurate estimation of the previously estimated paths, and the comparison value as an auxiliary judgment is used to estimate the remaining paths until enough paths are estimated. Simulation results show that our proposed scheme can effectively eliminate noise interference, while offering better estimation accuracy for the fast-changing channel scenario. We summarize the main contributions of this paper as follows:

- In the mmWave massive MIMO V2X fast vehicle communication system, a novel noise elimination-based DFT channel estimation scheme, called the NE-DFT channel estimation scheme is proposed to capture the channel state changes. Compared with the traditional DFT-CEA, the NE-DFT algorithm can effectively improve the channel estimation accuracy and significantly reduce noise interference.
- We first deploy a conventional DFT-CEA to initially estimate all channel path parameters. Second, a threshold is proposed to determine the authenticity of the channel paths estimated by DFT-CEA. Then, the energy distribution of the channel paths is analyzed, and submatrices are designed for energy extraction. Furthermore, the comparison parameter between the total energy of the channel matrix and the energy of the actual signal matrix is calculated, which are used as an auxiliary decision for the estimated paths whose energy is lower than a threshold. The paths with the smallest comparison values are selected in turn until the expected number of paths is estimated. Finally, the channel matrix is reconstructed using estimated channel parameters.
- The simulation results show that the estimation accuracy of the proposed NE-DFT algorithm is higher than that of the conventional channel estimation algorithms-based DFT (DFT-CEA). Furthermore, the complexity analysis of the proposed scheme shows that the proposed NE-DFT algorithm achieves lower computational complexity.

The rest of the paper is organized as follows. In Section II, the system model of channel estimation for the mmWave massive MIMO dynamic communication system is presented. In Section III, we introduce the proposed NE-DFT channel estimation scheme and analyze its performance. We present the simulation results in Section IV. Finally, we draw the conclusions in Section V.

Notation: Throughout this paper, vectors and matrices will be represented by boldfaced lower-case and upper-case letters (e.g., $\mathbf{a}$ and $\mathbf{A}$), respectively. Variables and constants are denoted in lower-case and upper-case letters (e.g., a and $\mathbf{A}$), respectively. $\mathbf{A}^T$, $\mathbf{A}^H$, $\mathbf{A}^{-1}$ and $\|\mathbf{A}\|$ represent the transpose, conjugate transpose, inverse, and Frobenius norm of $\mathbf{A}$, respectively; $|a|$ denotes the amplitude of a; $diag(a_1, \ldots, a_N)$ represents a block diagonal matrix whose diagonal entries are given by $\{a_1, \ldots, a_N\}$; $\left[\mathrm{y}\right]_{a:b}$ denotes a vector obtained by extracting elements of vector y from index a to index b; $\mathbf{0}_{N\times M}$ denotes a zero matrix of $N \times M$ size; $\mathcal{CN}(u, R)$ is a complex Gaussian random vector with the mean u and covariance R matrix; $I_N \in {}^{N\times N}$ denotes an $N \times N$ identity matrix and $\lceil a \rceil$ denotes the smallest integer not smaller than a; and $\mathbb{E}[X]$ denotes the expectation of the random X.

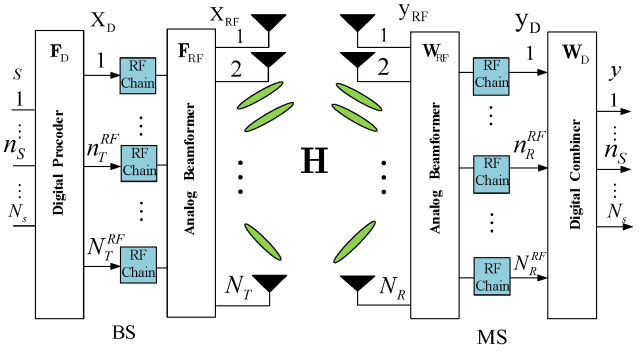

FIGURE 2. Block diagram of mmWave communication system.

II. SYSTEM MODEL

In this paper, we consider the downlink of the mmWave V2X fast vehicle communication system, as shown in Fig. 2. Due to a small number of effective scatters at mmWave frequencies, the rank of the MIMO channel matrix for each user is low, and the optimal number of data streams is much smaller than the number of antennas. Moreover, since the minimum number of RF chains is determined by the number of streams, the number of RF chains can be significantly reduced by the hybrid architecture, leading to reduce cost and energy consumption. In addition, although CSI is essential to benefit from the array gain provided by multiple antennas, it is challenging to acquire CSI in mobile networks when the channel changes rapidly. Thus, we need to consider a reasonable multistream system. We assume that there are L scattering clusters between BS and MS, and there is only one propagation path in each scattering cluster. The BS and MS are equipped with N_T transmitting antennas and N_R receiving antennas, respectively. We assume that the RF chains in BS are N_T^{RF} ($N_T^{RF} \leq N_T$) and the RF chains in MS are N_R^{RF} ($N_R^{RF} \leq N_R$). The transmitter and receiver are equipped with the same array architectures [12].

In the BS, the transmitted signal s is first processed in the digital precoder; next, we have that $\mathrm{x_D} = \mathbf{F_D}s$ where $\mathbf{F_D} \in \mathbb{C}^{N_T^{RF}\times N_s}$ is the baseband precoding matrix. Then, the new transmitted signal vector $\mathrm{x_D}$ is processed in the

analog beamformer, and we have that $x_{RF} = \mathbf{F}_{RF}x_D$ where $\mathbf{F}_{RF} \in \mathbb{C}^{N_T \times N_T^{RF}}$ is the precoding matrix. Thus, the precoder at BS is denoted as $\mathbf{F} = \mathbf{F}_{RF}\mathbf{F}_D \in \mathbb{C}^{N_T \times N_s}$. Similarly, $\mathbf{W}_{RF} \in \mathbb{C}^{N_R \times N_R^{RF}}$ is the RF combiner matrix, $\mathbf{W}_D \in \mathbb{C}^{N_R^{RF} \times N_s}$ is the baseband combination matrix, and the combiner at MS is $\mathbf{W} = \mathbf{W}_{RF}\mathbf{W}_D \in \mathbb{C}^{N_R \times N_s}$.

We adopt a narrowband block-fading channel model; at the receiver we observe the following:

$$y_{RF} = \mathbf{H}\mathbf{F}_{RF}x_D + \mathbf{n}, \tag{1}$$

where $\mathbf{n} \sim \mathcal{CN}(\mathbf{0}_{N_R \times 1}, \sigma^2\mathbf{I}_{N_R})$ is the Gaussian noise with variance σ^2 imposed on the received signal. Furthermore, if the RF combiner matrix $\mathbf{W}_{RF}$ is applied to the received signal y_{RF}, the processed received signal can be written as

$$y_D = \mathbf{W}_{RF}^H y_{RF} = \mathbf{W}_{RF}^H(\mathbf{H}\mathbf{F}_{RF}x_D + \mathbf{n}), \tag{2}$$

and the final processed data at the MS is $\mathbf{y} = \mathbf{W}_D\mathbf{y}_D$. The received signal at the MS can be expressed as

$$\mathbf{Y} = \mathbf{W}^H\mathbf{H}\mathbf{F}s + \mathbf{W}^H\mathbf{n}, \tag{3}$$

where $\mathbf{H} \in \mathbb{C}^{N_R \times N_T}$ denotes the mmWave channel matrix between the BS and MS.

Assuming a uniform linear array (ULA) at both ends of the transmission, the channel matrix $\mathbf{H}$ can be expressed as

$$\mathbf{H} = \frac{1}{\sqrt{L}}\sum_{1}^{L}\rho_l\alpha_{MS}\left(\varphi_l^r\right)\alpha_{BS}^H\left(\theta_l^t\right), \tag{4}$$

where $\rho_l \sim \mathcal{CN}(0,1)$, $l = 1, 2, \ldots, L$ is the complex gain of the l^{th} path between BS and MS. $\theta_l^t \in [0, 2\pi]$ and $\varphi_l^r \in [0, 2\pi]$ denote the azimuth angles of departure (AODs) and the azimuth angles of arrival (AOAs) between BS and MS, respectively. $\alpha_{BS}\left(\theta_l^t\right)$ and $\alpha_{MS}(\varphi_l^r)$ are the antenna array response vectors at BS and MS, respectively. Using a ULA, $\alpha_{BS}\left(\theta_l^t\right)$ can be expressed as

$$\alpha_{BS}\left(\theta_l^t\right) = \left[1, e^{j(\frac{2\pi}{\lambda})d\sin(\theta_l^t)}, \ldots, e^{j(\frac{2\pi}{\lambda})(N_T-1)d\sin(\theta_l^t)}\right]^T, \tag{5}$$

where λ is the signal wavelength corresponding to the operating carrier frequency and d is the inter-element distance of antenna elements which is assumed $d = \lambda/2$. Similarly, the direction vector of MS, $\alpha_{MS}(\varphi_l^r)$, can be obtained. The channel in (4) is written in a more compact form as

$$\mathbf{H} = \frac{1}{\sqrt{L}}\mathbf{A}_{MS}\mathbf{H}_\rho\mathbf{A}_{BS}^H \tag{6}$$

with

$$\mathbf{H}_\rho = diag(\rho), \rho = [\rho_1, \rho_2, \ldots, \rho_L]^T \in \mathbb{C}^{N_R \times N_T}, \tag{7}$$

$$\mathbf{A}_{MS} = \left[\alpha_{MS}(\varphi_1^r), \alpha_{MS}(\varphi_2^r), \ldots, \alpha_{MS}(\varphi_l^r)\right], \tag{8}$$

$$\mathbf{A}_{BS} = \left[\alpha_{BS}(\theta_1^t), \alpha_{BS}(\theta_2^t), \ldots, \alpha_{BS}(\theta_l^t)\right], \tag{9}$$

where (8) and (9) contain received and transmitted angle parameters of all paths, respectively.

III. CHANNEL ESTIMATION ALGORITHM BASED ON NE-DFT

Since users move fast in mmWave vehicle communication, the signals of users are greatly interfered by noise and the communication quality is deteriorated. Thus, the number of channel paths estimated by the conventional estimation method cannot maintain the normal vehicle communication. To address this problem, we need to estimate more channel paths and reduce noise interference.

In this section, inspired by the idea of the iterative cancellation conceived for channel estimation [20], namely, the DFT-CEA, we propose a novel channel estimation scheme called NE-DFT to support users under mobility, which significantly reduces noise interference, improves channel estimation accuracy, and makes it a viable algorithm for mmWave massive MIMO vehicular cellular scenarios. First, the conventional DFT-CEA is employed to initially estimate all path parameters. Next, a judgment threshold based on noise energy is proposed to improve the accuracy of each path that has been estimated. Then, the comparison between the channel submatrix and the standard submatrix is calculated, and the path with the smallest comparison value is selected from the remaining paths as the actual path. Additionally, based on the comparison value, an auxiliary judgment is developed to estimate enough real paths. Finally, the channel matrix is reconstructed by using estimated channel parameters. The pieces are put together by explaining our proposed NE-DFT algorithm.

A. PARAMETER ESTIMATION OF THE PATH BASED ON THE CONVENTIONAL DFT-CEA

The received signals of all antennas cannot be extracted simultaneously; therefore, the channel estimations are more complicated in a hybrid mmWave architecture. Moreover, the conventional channel estimation algorithms are not feasible due to the constraint of analog beamformers and the numerous transmit/receive antennas that require a very long training sequence. In Part A, to address the shortcomings of the traditional schemes, we deploy the conventional DFT-CEA to initially estimate all parameters of channel paths. Specifically, a training sequence that includes a set of analog and digital beamformers is used to probe the channel. By exploiting the scattering of the mmWave channel, Algorithm 1 is developed to leverage the 2D-DFT of the received training samples, and iteratively estimate AOA θ_l^t, AOD φ_l^r and gain ρ_l of the different scatters.

In the mmWave massive MIMO vehicular cellular system, the massive MIMO techniques provide a large space diversity. Due to the large number of antennas, $\mathbf{H}$ can achieve a larger dimension, which is up to hundreds of columns and rows and depends on the number of antennas. However, since the channel paths L are usually much smaller than the number of antennas, i.e., only L elements of $\mathbf{H}$ are nonzeros, $\mathbf{H}$ is a spare matrix. Thus, for the channel estimation of the mmWave massive MIMO vehicular cellular system, we only need to

estimate $2L$ angles and L complex gains to construct the entire channel matrix. We estimate the entire channel parameters by estimating a portion submatrix $\tilde{\mathbf{H}}$ of the channel matrix $\mathbf{H}$ [20], [21], and from (6) we can construct the estimation matrix for the entire channel $\hat{\mathbf{H}}$. For simple analysis, we can define the following:

$$\Phi_l^t = (2\pi/\lambda)d\sin(\theta_l^t), \tag{10}$$
$$\Phi_l^r = (2\pi/\lambda)d\sin(\varphi_l^r), \tag{11}$$

the $(n, m) - th$ element of the channel matrix $\mathbf{H}$ is defined as follows:

$$[\mathbf{H}]_{n,m} = \frac{1}{\sqrt{L}}\sum_{l=1}^{L}\rho_l e^{jn\Phi_l^r}e^{-jm\Phi_l^t}, \tag{12}$$

where $n = 0, 1, 2, \cdots, N_R - 1$ and $m = 0, 1, 2, \cdots, N_T - 1$. From (12), each element of $\mathbf{H}$ is a superposition of L complex numbers, and each of complex numbers is determined by path parameter $\rho_l, \theta_l^t, \varphi_l^r$. Thus, the channel parameters can be estimated by performing two dimensional DFT (2D-DFT) processing on the channel matrix $\mathbf{H}$.

From (6), each element of $\mathbf{H}$ contains all the path parameters information; we extract a part of submatrix $\tilde{\mathbf{H}}$ of $\mathbf{H}$ and extract the required parameter information from $\tilde{\mathbf{H}}$. We define the $N_R^d \times N_T^d$ submatrix as follows:

$$\mathbf{H} = [\mathbf{H}]_{0:N_R^d-1,0:N_T^d-1}, \tag{13}$$

where

$$N_R^d \le N_R, \quad N_R^d = sN_R^{RF}, \tag{14}$$
$$N_T^d \le N_T, \quad N_T^d = tN_T^{RF}, \tag{15}$$

where N_R^d and N_T^d are two suitable integer parameters to be chosen depending on the length N_{TS} of the training sequence. Matrix $\tilde{\mathbf{H}}$ can be obtained by stacking the following $N_R^{RF} \le N_T^{RF}$ submatrix blocks:

$$\mathbf{H}^{(s,t)} = [\tilde{\mathbf{H}}]_{sN_R^{RF}:(s+1)N_R^{RF}-1,tN_T^{RF}:(t+1)N_T^{RF}-1}, \tag{16}$$

where

$$s = 0, 1, 2, \cdots, \left\lceil N_R^d/N_R^{RF}\right\rceil - 1, \tag{17}$$
$$t = 0, 1, 2, \cdots, \left\lceil N_T^d/N_T^{RF}\right\rceil - 1. \tag{18}$$

To estimate $\tilde{\mathbf{H}}^{(s,t)}$, BS sends some training sequences, i.e., the column vector $\mathbf{x}_{\mathrm{D}}^{(m)}, m = 0, 1, 2, \cdots, N_T^{RF} - 1$ to MS, where $\mathbf{x}_{\mathrm{D}}^{(m)}$ has $1/\sqrt{N_T^{RF}}$ in position m and zero otherwise. For each of these sequences, we design the analog transmit beamformer $\mathbf{F}_{\mathrm{RF}}^{(t)}$ to switch on only transmit antennas $tN_T^{RF}, \ldots, (t+1)N_T^{RF} - 1$, i.e., we set

$$\mathbf{F}_{\mathrm{RF}}^{(t)} = \begin{bmatrix} \mathbf{0}_{tN_T^{RF}\times N_T^{RF}} \\ \bar{\mathbf{F}}_{\mathrm{RF}} \\ \mathbf{0}_{(N_T-(t+1)N_T^{RF})\times N_T^{RF}} \end{bmatrix}, \tag{19}$$

where $\bar{\mathbf{F}}_{\mathrm{RF}}$ is a $N_T^{RF} \times N_T^{RF}$ square matrix, whose elements are chosen with unitary magnitude and arbitrary phases, and such that $\bar{\mathbf{F}}_{\mathrm{RF}}$ has full rank. Meanwhile, we design the analog receive beamformer by switching on only receive antennas $sN_R^{RF}, \ldots, (s+1)N_R^{RF} - 1$, i.e., we set

$$\mathbf{W}_{\mathrm{RF}}^{(s)} = \begin{bmatrix} \mathbf{0}_{sN_R^{RF}\times N_R^{RF}} \\ \bar{\mathbf{W}}_{\mathrm{RF}} \\ \mathbf{0}_{(N_R-(s+1)N_R^{RF})\times N_R^{RF}} \end{bmatrix}, \tag{20}$$

where $\bar{\mathbf{W}}_{\mathrm{RF}}$ is a $N_R^{RF} \times N_R^{RF}$ full rank square matrix, whose elements have unitary magnitude and arbitrary phases. From (2), the baseband signal at BS becomes

$$\begin{aligned}\mathbf{y}_{\mathrm{D}}^{(s,t,m)} &= (\mathbf{W}_{\mathrm{RF}}^{(s)})^H(\mathbf{H}\mathbf{F}_{\mathrm{RF}}^{(t)}\mathbf{x}_{\mathrm{D}}^{(m)} + \mathbf{n}^{(m)}) \\ &= \bar{\mathbf{W}}_{\mathrm{RF}}^H(\tilde{\mathbf{H}}^{(s,t)}\bar{\mathbf{F}}_{\mathrm{RF}}\mathbf{x}_{\mathrm{D}}^{(m)} + \bar{\mathbf{n}}^{(m)}),\end{aligned} \tag{21}$$

where $m = 0, 1, 2, \cdots, N_T^{RF} - 1$, and

$$\bar{\mathbf{n}}^{(m)} = [\bar{\mathbf{n}}^{(m)}]_{sN_R^{RF}:(s+1)N_R^{RF}-1}. \tag{22}$$

After all sequences $\mathbf{x}_{\mathrm{D}}^{(0)}, \mathbf{x}_{\mathrm{D}}^{(1)}, \cdots, \mathbf{x}_{\mathrm{D}}^{(N_T^{RF}-1)}$ spread over the wireless channel, the receiver signal in MS is defined as

$$\mathbf{Y}_{\mathrm{D}}^{(s,t)} = [\mathbf{y}_{\mathrm{D}}^{(s,t,0)}, \mathbf{y}_{\mathrm{D}}^{(s,t,1)}, \cdots, \mathbf{y}_{\mathrm{D}}^{(s,t,N_T^{RF}-1)}]. \tag{23}$$

Then, based on (21) and (23), we can achieve the estimated submatrix blocks

$$\begin{aligned}\hat{\tilde{\mathbf{H}}}^{(s,t)} &= \sqrt{N_T^{RF}}(\bar{\mathbf{W}}_{\mathrm{RF}}^H)^{-1}\mathbf{Y}_{\mathrm{D}}^{(s,t)}(\bar{\mathbf{F}}_{RF})^{-1} \\ &= \tilde{\mathbf{H}}^{(s,t)} + \tilde{\mathbf{n}},\end{aligned} \tag{24}$$

where $\tilde{\mathbf{n}} = \sqrt{N_T^{RF}}\left[\bar{\mathbf{n}}^{(0)}, \bar{\mathbf{n}}^{(1)}, \ldots, \bar{\mathbf{n}}^{(N_T^{RF}-1)}\right](\bar{\mathbf{F}}_{RF})^{-1}$.

To ensure the full rank of matrices $\bar{\mathbf{F}}_{\mathrm{RF}}$ and $\bar{\mathbf{W}}_{\mathrm{RF}}$, we employ the Hadamard matrices. This guarantees that the noise in (24) is still white with variance σ^2. An estimated submatrix $\hat{\tilde{\mathbf{H}}}$ of the estimation matrix for the entire channel $\hat{\mathbf{H}}$ can be obtained by stacking several the estimated submatrix blocks $\hat{\tilde{\mathbf{H}}}^{(s,t)}$ in (24).

To estimate the parameters ρ_l, θ_l^t, φ_l^r, $l = 1, 2, \ldots, L$ of the L complex modes, we compute the 2D-DFT of $\hat{\tilde{\mathbf{H}}}$ on $N_{DFT} \times N_{DFT}$ samples, which can derived as follows:

$$W(k,i) = \sum_{m=0}^{N_T^d-1}\sum_{n=0}^{N_R^d-1}[\hat{\tilde{\mathbf{H}}}]_{n,m}e^{-j2\pi(im+kn)/N_{DFT}}, \tag{25}$$

for $k, i = 0, 1, \ldots, N_{DFT} - 1$.

Let $\mathbf{R}(n, m)$ denote a matrix with elements being one

$$\mathbf{R}(n,m) = \begin{cases} 1, & 0 \le n < N_R^d, 0 \le m < N_T^d, \\ 0, & \text{otherwise}, \end{cases} \tag{26}$$

and its DFT is given by

$$R(k,i) = \sum_{m=0}^{N_T^d-1}\sum_{n=0}^{N_R^d-1}e^{-j2\pi(im+kn)/N_{DFT}}. \tag{27}$$

Uniform quantized Φ_l^t and Φ_l^r, then we have the following:

$$\Phi_l^t = -\frac{2\pi i_l}{N_{DFT}}, \tag{28}$$

$$\Phi_l^r = \frac{2\pi k_l}{N_{DFT}}. \tag{29}$$

Simplify (12), (27)-(29), (25) can be rewritten as

$$W(k,i) = \frac{1}{\sqrt{L}} \sum_{l=1}^{L} \rho_l R(k-k_l, i-i_l) + \tilde{N}(k,i), \tag{30}$$

where $k, i = 0, 1, 2, \cdots, N_{DFT} - 1$ and $\tilde{N}(k,i) \in \mathcal{CN}(0, N_R^d N_T^d \sigma^2)$ is a noise matrix. According to formula (30), the iterative cancellation method is adopted to estimate the channel parameters of the different modes in Algorithm 1. To be specific, by indicating with $W_l(k,i)$ the 2D-DFT of the channel matrix obtained by removing the first $l-1$ estimated modes, at iteration l, we first estimate the index $(\hat{k}_l, \hat{i}_l)$ that maximize $|W_l(k,i)|$, i.e.,

$$(\hat{k}_l, \hat{i}_l) = \arg\max_{k,i} |W_l(k,i)|. \tag{31}$$

Then, the AOA and AOD of the l^{th} ray can be computed by (10), (11) and (28), as well as (29), so we have the following:

$$\hat{\theta}_l^t = \sin^{-1}(-2\hat{i}_l/N_{DFT}), \tag{32}$$

$$\hat{\varphi}_l^r = \sin^{-1}(2\hat{k}_l/N_{DFT}), \tag{33}$$

from (30), the complex gain turns out to be

$$\hat{\rho}_l = W_l(\hat{k}_l, \hat{i}_l)\sqrt{L}/(N_R^d N_T^d), \tag{34}$$

after estimating all channnel parameters $\hat{\rho}_l$, $\hat{\varphi}_l^r$, $\hat{\theta}_l^t$, from (6) we can construct the estimation matrix for the entire channel $\hat{\mathbf{H}}$.

Channel estimation is needed to fully benefit from the beamforming and obtaining a reliable channel estimation has been recognized as one of the main challenges. However, since the channel is time-varying in a fast manner in the high-speed scenario, the estimation accuracy of the iterative cancellation method may decrease with the change of the channel state. The point selected by the iterative cancellation method may not be the real path in (31); it could be noise jamming. Therefore, we need to improve the defects of Algorithm 1.

Given that in time-varying channels, the accuracy of channel estimation is mainly the interference of noise, if the noise interference can be effectively eliminated, the problem in Algorithm 1 can be solved. Thus, if the characteristics of the noise in $|W_l(k,i)|$ are known, we can eliminate the noise from the real paths and determine the reliability of the paths. In the following, to distinguish the noise, a strategy will be proposed to judge the reliability of the estimated paths.

B. A STRATEGY OF REAL PATH JUDGMENT

In the mmWave vehicle communications, the channel of users deteriorates at every moment due to the rapid movement of the users, which leads to the signal gain becoming weaker during the propagation of signals. Thus, the conventional channel estimation schemes encounter difficulty in obtaining the ideal estimation accuracy, especially when serious noise interference exists. Additionally, the DFT-CEA in Part A is only suitable for static or slowly time-variant scenarios; the paths estimated by the conventional channel estimation algorithms may be misjudged when in the fast time-variant channel. Then, we need to analyze the distribution characteristics of the noise and useful signals in the channel as well as their relationship when the signals are severely disturbed by noise. To address the problems, we set a threshold based on the noise energy to judge the real paths estimated by the DFT-CEA in Part A.

Algorithm 1 The Iterative Cancellation Method to Estimate the Channel

Input: BS and MS know $N_T, N_R, N_T^{RF}, N_R^{RF}, L, N_{DFT}$;
Output: Matrix $\mathbf{H} \in \mathbb{C}^{N_R \times N_T}$;
Initialization: $N_T^d = N_T^{RF}, N_R^d = N_R^{RF}$;
1: BS sends $\mathbf{x}_{\mathrm{D}}^{(m)}$ and uses $\mathbf{F}_{\mathrm{RF}}^{(t)}$, MS uses $\mathbf{W}_{\mathrm{RF}}^{(s)}$
2: calculate $\hat{\tilde{\mathbf{H}}}^{(s,t)}$ and stack them $\hat{\tilde{\mathbf{H}}}$
3: $W_1(k,i) = W(k,i)$
4: for $l = 1$ to L_d
5: $(\hat{k}_l, \hat{i}_l) = \arg\max_{k,i} |W_l(k,i)|$
6: $\hat{\rho}_l = W_l(\hat{k}_l, \hat{i}_l)\sqrt{L}/(N_R^d N_T^d)$
7: $W_{l+1}(k,i) = W_l(k,i) - \hat{\rho}_l R(k-k_l', i-i_l')/\sqrt{L}$
8: $\hat{\theta}_l^t = \sin^{-1}(-2\hat{i}_l/N_{DFT})$, $\hat{\varphi}_l^r = \sin^{-1}(2\hat{k}_l/N_{DFT})$
9: end

Estimating the submatrix from equation (24) based on above analyses, it is expressed as

$$\hat{\tilde{\mathbf{H}}} = \tilde{\mathbf{H}} + \tilde{\mathbf{n}}, \tag{35}$$

where $\tilde{\mathbf{H}}$ is the real path, and $\tilde{\mathbf{n}} \in \mathbb{C}^{N_R^d \times N_T^d}$ is a noise matrix whose elements are i.i.d. and it obeys the Gaussian distribution $\mathcal{CN}(0, \sigma^2)$. Substituting (35) into (25), we have the following:

$$\begin{aligned} W(k,i) &= \sum_{m=0}^{N_T^d-1} \sum_{n=0}^{N_R^d-1} ([\tilde{\mathbf{H}}]_{n,m} + [\tilde{\mathbf{n}}]_{n,m}) e^{-j2\pi(im+kn)/N_{DFT}} \\ &= \sum_{m=0}^{N_T^d-1} \sum_{n=0}^{N_R^d-1} [\tilde{\mathbf{H}}]_{n,m} e^{-j2\pi(im+kn)/N_{DFT}} \\ &\quad + \sum_{m=0}^{N_T^d-1} \sum_{n=0}^{N_R^d-1} [\tilde{\mathbf{n}}]_{n,m} e^{-j2\pi(im+kn)/N_{DFT}} \\ &= H(k,i) + \tilde{N}(k,i), \end{aligned} \tag{36}$$

where $\tilde{N}(k,i)$ is the noise matrix after 2D-DFT processing, and each element obeys a complex Gaussian distribution $\tilde{N}(k,i) \in \mathcal{CN}(0, N_R^d N_T^d \sigma^2)$, and the modulus $\left|\tilde{N}(k,i)\right|$ of noise $\tilde{N}(k,i)$ obeys the Rayleigh distribution whose cumulative distribution function is as follows:

$$F(x) = 1 - e^{-x^2/2N_T^d N_R^d \sigma^2}, \quad x \geq 0. \tag{37}$$

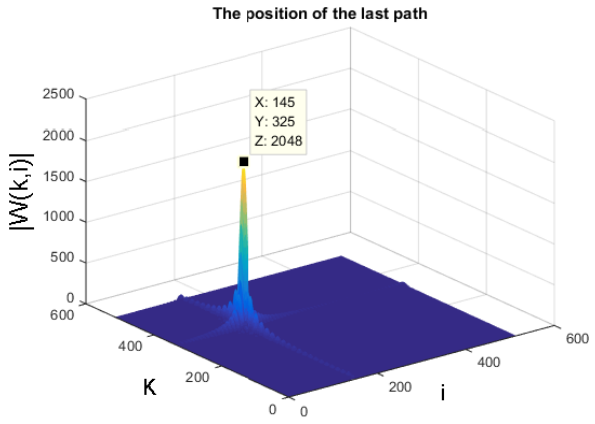

FIGURE 3. The position of the last path.

According to the sparse nature of the mmWave channel, i.e., only the angles (AOAs and AODs) at the real paths have a large energy, the energy in the remaining angle is close to zero. $|H(k,i)|, k, i = 0, 1, 2, \cdots, N_{DFT} - 1$ is a matrix whose angle of the path corresponds to a position with a larger value, and the value of other positions is approximately zero. The position of the path presents an "energy peak", as shown in Fig. 3.

According to the distribution characteristics of $|H(k,i)|$ and $\left|\tilde{N}(k,i)\right|$, from (36) we can obtain

$$\begin{aligned} |W(k,i)| &= \left|H(k,i) + \tilde{N}(k,i)\right| \\ &\approx |H(k,i)| + \left|\tilde{N}(k,i)\right|, \end{aligned} \tag{38}$$

if we know the characteristics of noise $\left|\tilde{N}(k,i)\right|$ within $|W(k,i)|$, $|H(k,i)|$ and $\left|\tilde{N}(k,i)\right|$ can be distinguished; then, the reliability of the estimated path is decided.

Based on [20], the point of the maximum energy can be found from (38) as follows:

$$\begin{aligned} (\hat{k}_l, \hat{i}_l) &= \max_{k,i} |W(k,i)| \\ &\approx \max_{k,i} \end{aligned} \tag{39}$$

to guarantee the accuracy of the estimation. The noise interference should be eliminated as much as possible, in other words, the energy of the selected point $\left|W(\hat{k}_l, \hat{i}_l)\right|$ should be greater than that of the noise interference $\left|\tilde{N}(k,i)\right|$, i.e.,

$$\left|W(\hat{k}_l, \hat{i}_l)\right| > \max_{k,i} \left|\tilde{N}(k,i)\right|. \tag{40}$$

Eq. (40) is the condition for determining whether the path is a real path. However, it is difficult to meet (40); therefore, we replace $\max_{k,i} \left|\tilde{N}(k,i)\right|$ with a threshold δ_{thres}, and (40) can be rewritten as

$$\left|W(\hat{k}_l, \hat{i}_l)\right| > \delta_{thres}. \tag{41}$$

Since $\left|\tilde{N}(k,i)\right|$ is a random variable that obeys the Rayleigh distribution, and according to (37), let $x_0 = 3\sigma\sqrt{N_T^d N_R^d}$; then, (37) can be rewritten as

$$F(x_0) = 1 - e^{-{x_0}^2/2N_T^d N_R^d \sigma^2} = 0.988 \to 1, \tag{42}$$

let x_0 be a proper threshold. To fine-tune the threshold, an adjustable coefficient η is set as follows:

$$\delta_{thres} = \eta x_0, \tag{43}$$

where η is a variable with a value close to 1. Based on (41), (42) and (43), we can achieve the following:

$$\left|W(\hat{k}_l, \hat{i}_l)\right| > \delta_{thres} = 3\eta\sigma\sqrt{N_R^d N_T^d}. \tag{44}$$

Then, we can determine the reliability of paths estimated by Part A based on (44). In other words, if the estimated paths satisfy condition (44), the estimated paths are considered to exist; otherwise, the estimated paths are considered unreliable.

C. ANALYSIS OF PATH ENERGY DISTRIBUTION AND DESIGN OF SUBMATRIX FOR EXTRACTING ENERGY

In Part B, we proposed the channel estimation method to effectively judge the real paths whose energy is greater than the threshold δ_{thres}. However, the signals are susceptible to noise because the communication channels in the vehicle cellular systems are time-varying. In particular, it is difficult to effectively estimate the actual path by using the judgment method of Part B when the energy of some paths is lower than the threshold δ_{thres}, i.e., $\left|W(\hat{k}_l, \hat{i}_l)\right| < \delta_{thres}$. Therefore, the estimated parameters $\rho_l, \theta_l^t, \varphi_l^r, l = 1, 2, \ldots, L$ of the L paths may not be accurate enough, especially the paths with a smaller gain that may be submerged in the noise, resulting in misjudgment of the channel estimation in the previous step. To estimate the channel paths whose energy is less than threshold δ_{thres}, we need to extract energy and then perform a comparison operation. Thus, the energy distribution of each path and its own adjacent paths is need to analyzed before the path energy is extracted. An appropriate submatrix for energy extraction is designed to avoid extracting the energy of adjacent paths when the energy of the estimated path is extracted. In particular, the number of channel paths judged by the channel estimation method in Part B may not have reached the expected number of paths. Therefore, we need to select enough paths from the remaining paths whose energy is lower than threshold δ_{thres}, which to reach the expected number of paths.

Next, the analysis of the path energy distribution is given to design the submatrix for extracting energy. To avoid extracting energy from the adjacent paths, we analyze the approximate power distribution of each path, and the relationship between the energy distributions of the estimated paths and that of adjacent paths.

1) THE ANALYSIS OF THE SINGLE PATH CASE

The 2D-DFT of the estimation submatrix of the channel $\hat{\tilde{\mathbf{H}}}$ is defined as $W(k, i)$. Most of the power for $W(k, i)$ concentrates around (k_l', i_l'). Specifically, $W(k, i)$ only has one nonzero point (k_l', i_l') as $k \to \infty, i \to \infty$.

The author of [26] has analyzed the energy distribution of the path in the mmWave channel, proving that the most of energy of all single channel paths was concentrated on one point, and the energy of each channel path did not overlap with each other. Similar to [26], ULA is used in our algorithm, the sparsity of the path and the distribution characteristics of the main channel energy have been proven. An example for the position of the last path is illustrated in Fig. 3, in which 2D-DFT is depicted with $N_{DFT} \times N_{DFT} = 512 \times 512$, and the number of transmitting and receiving antennas are $M = 128$ and $N = 64$, respectively. As shown in Fig. 3, it can be checked that the central point of the channel after 2D-DFT is (145, 325, 2048). Most of the power concentrates around points (k_l', i_l'), and the position and height of the "energy peak" correspond to the angle parameters and the path gain, respectively.

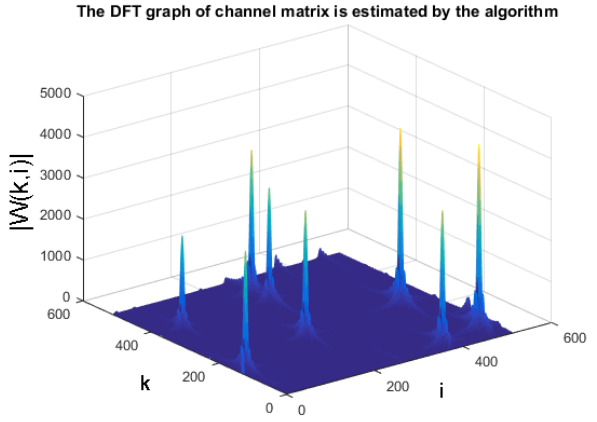

FIGURE 4. The DFT graph of the channel matrix is estimated by the algorithm.

2) THE ANALYSIS OF THE MULTIPATH CASE

From the above analysis, the most of power for each channel path concentrated around a point in their own paths after the channel matrix is processed by 2D-DFT. This analysis provides theoretical support for the proposed scheme to extract the main energy of the path at point (k_l', i_l'). The DFT graph of the channel matrix estimated by the proposed algorithm is shown in Fig. 4. We can see that the energy of each path is almost concentrated at its own point (k_l', i_l'), and the path "peak" is far from the adjacent path "peak", namely, the energy of all paths does not overlap with each other. Moreover, the lowest point (i, j) of the groove is taken as the boundary between the two adjacent paths. Additionally, a submatrix $\tilde{\mathbf{W}}$ with dimension $N_R^{sub} \times N_T^{sub}$ is designed to extract the most power from the path $W(k, i)$ at point (k_l', i_l'). Similarly, a submatrix $\tilde{\mathbf{R}}$ with the dimension $N_R^{sub} \times N_T^{sub}$ is used to extract the most power from the signal $H(k, i)$ at point (k_l', i_l'), where N_R^{sub} and N_T^{sub} are the row and column of the submatrix, respectively. Thus, the energy of the adjacent path will not be extracted when we extract the most power at point (k_l', i_l'), and misjudgment does not occur.

Although two paths are very close with a small probability, misjudgment can still occur. d is the distance between two adjacent paths in which the energy is lower than threshold δ_{thres}. $d/2$ is the distance between point (i, j) and point (k_l', i_l'), where point (i, j) is the boundary of two adjacent paths, i.e., the point (i, j) is where we extract the maximum path energy.

I: $d/2$ is greater than the maximum dimension $\max\left\{N_R^{sub}, N_T^{sub}\right\}$ of the energy submatrix when we extract energy at point (k_l', i_l'), i.e., $\frac{d}{2} \geq \max\left\{N_R^{sub}, N_T^{sub}\right\}$. The two paths can be distinguished when we extract the most of power from the path with strong energy, and the energy of the adjacent path with weak gain is not extracted.

II: d is smaller than the minimum dimension $\min\left\{N_R^{sub}, N_T^{sub}\right\}$ of the energy submatrix when the two paths are very close, i.e., $d \leq \min\left\{N_R^{sub}, N_T^{sub}\right\}$. As shown in Fig. 5, the signals are completely submerged by noise, we consider them to belong to the same path, and the energy extraction can be achieved by the proposed algorithm.

3) DESIGN OF SUBMATRIX DIMENSIONS

The dimensions of submatrix $\tilde{\mathbf{W}}$ and submatrix $\tilde{\mathbf{R}}$ are all $N_T^{sub} \times N_R^{sub} = 19 \times 9$, and $\tilde{\mathbf{W}}$ and $\tilde{\mathbf{R}}$ are used to extract the energy of the path and signal at (k_l', i_l'), respectively. To effectively estimate the channel, the number of rows and columns of the submatrix should be greater than the number of RF chains in the transmitter and the number of RF chains in the receiver, respectively. The minimum number of rows or columns for the submatrix must be greater than the minimum number of RF chains in either the transmitter or the receiver, i.e., $\min\left\{N_T^{sub}, N_R^{sub}\right\} > \min\left\{N_T^{RF}, N_R^{RF}\right\}$. Therefore, we can ensure that under the premise of extracting the main energy around the point (k_l', i_l'), the range of the submatrix for extracting energy does not exceed the lowest point (i, j) of the groove.

D. JUDGE THE AUTHENTICITY OF THE ESTIMATED PATHS

From the above analyses, it is difficult to accurately estimate the path using the channel estimation method in Part B when $\left|W(\hat{k}_l, \hat{i}_l)\right| < \delta_{thres}$. In particular, the number of paths judged by the estimation method in Part B cannot reach the expected total number of paths, so enough paths from the remaining paths whose energy is lower than threshold δ_{thres} are selected, which reach the expected total number of paths. Moreover, in part C, we analyze the main energy distribution of all paths and give the design of the submatrix for extracting path energy, which are used to judge the authenticity of the remaining paths. To compensate for the shortcomings of Part B, the matrix for extracting energy is exploited and a comparison operation is performed to estimate the sufficient

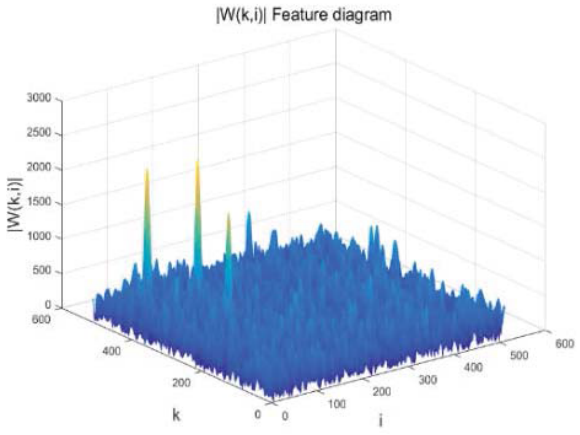

FIGURE 5. Instance diagram, $SNR = -6dB$, $L = 6$, $N_{DFT} = 512$, the "peaks" are actually paths with a larger gain and other paths with a smaller gain are submerged in noise.

number of paths from the remaining paths whose energy is less than threshold δ_{thres}, until the expected total numbers of estimated paths are reached.

According to the conclusion of [20], incorporating (30) and (36), $W(k, i)$ is decomposed into the following:

$$\begin{aligned} W(k,i) &= \frac{1}{\sqrt{L}} \sum_{l=1}^{L} \rho_l R(k-k_l, i-i_l) + \tilde{N}(k,i) \\ &= H(k,i) + \tilde{N}(k,i), \end{aligned} \tag{45}$$

where $k, i = 0, 1, 2, \cdots, N_{DFT} - 1$, and $R(k, i)$ is the 2D-DFT transform of the matrix with all elements being one. After the 2D-DFT processing on $W_l(k, i)$ in (45), the parameters are set as $SNR = -6dB$, $L = 6$, $N_{DFT} = 512$, and $|W_l(k, i)|$ as shown in Fig. 5, which presents a simulation example of $\left|W(\hat{k}_l, \hat{i}_l)\right|$; moreover, a few path directions with a larger path gain are clearly indicated by the 2D-DFT transform of $W_l(k, i)$. Since the number of L is generally much smaller than that of elements in $|W_l(k, i)|$, the channel matrix $|W_l(k, i)|$ can be modeled as a sparse matrix in the angular domain. The position and height of the "energy peak" correspond to the angle parameters and the path gain, respectively. Other paths with a smaller gain are submerged in noise. $\left|R(k-k'_l, i-i'_l)\right|$ presents a huge gain around (k'_l, i'_l), $\left|\tilde{N}(k,i)\right|$ obeys Rayleigh distribution; thus, $\frac{1}{\sqrt{L}}\rho'_l \left|R(k-k'_l, i-i'_l)\right|$ and $\left|\tilde{N}(k,i)\right|$ are superimposed, and $\left|W(\hat{k}_l, \hat{i}_l)\right|$ emerge as "energy peaks". The "energy peaks" of all paths are similar in shape, while the noise is irregular. The main energy of the region that is centered on (k'_l, i'_l) is extracted from $W_l(k, i)$ when path is estimated, and the submatrix $\tilde{\mathbf{W}}$ with the dimension $N_R^{sub} \times N_T^{sub}$ is obtained as follows:

$$\tilde{\mathbf{W}} = [W]_{k'_l - \frac{N_R^{sub}-1}{2} : k'_l + \frac{N_R^{sub}-1}{2}, i'_l - \frac{N_T^{sub}-1}{2} : i'_l + \frac{N_T^{sub}-1}{2}}, \tag{46}$$

the main energy of region is centered on (k'_l, i'_l) is extracted from matrix $\frac{1}{\sqrt{L}}\rho'_l \left|R(k-k'_l, i-i'_l)\right|$ when a real path exists at (k'_l, i'_l), and the submatrix $\tilde{\mathbf{R}}$ with the dimension $N_R^{sub} \times N_T^{sub}$ can be obtained. We define E_l as the auxiliary judgment parameter, and E_l represents similarity between $\tilde{\mathbf{W}}$ and $\tilde{\mathbf{R}}$. The similarity E_l is obtained by operation (47) between $\tilde{\mathbf{W}}$ and $\tilde{\mathbf{R}}$ as follows:

$$E_l = \left\|\tilde{\mathbf{W}} - \tilde{\mathbf{R}}\right\|^2 / \left\|\tilde{\mathbf{R}}\right\|^2, \tag{47}$$

By comparing the size of E_l, we can know the similarity between $\tilde{\mathbf{W}}$ and $\tilde{\mathbf{R}}$, i.e., the smaller E_l is, the more similar $\tilde{\mathbf{W}}$ and $\tilde{\mathbf{R}}$ are, which indicates that the existence of an actual path at (k'_l, i'_l) with greater probability. The E_l is used as a criterion for judging whether an actual path at (k'_l, i'_l) exists.

We first estimate the L_d ($L_d \geq L$) paths using the method of Part A when L paths need to be estimated; then, the scheme of Part B is used to determine S ($S \leq L$) paths where S is the number of paths satisfying (44). However, S has not yet reached the expected total number of paths L, so we need to select another $(L - S)$ paths from the remaining unreliable paths $(L_d - S)$ to reach the expected total number of estimated paths L. For this reason, E_l in operation (47) is performed on each of the remaining unreliable paths $(L_d - S)$, respectively. All the E_l values are in descending order, and the $(L - S)$ paths with the smallest E_l value are selected from the descending order of E_l as the actual paths, until the total estimated number of paths L are reached.

According to the above analyses, we judge the total L_d estimated paths to ensure the accuracy of all estimated L paths. Firstly, Part A is exploited to estimate enough paths, then we determine the reliability of paths that estimated by Part A based on (44). If the estimated paths satisfy condition (44), the paths are considered to exist, otherwise, the estimated paths are considered unreliable. Finally, we perform comparison operations one by one on the remaining paths that are judged to be unreliable. The paths with the smallest E_l are selected in the remaining paths until enough L paths are selected. The channel matrix $\mathbf{H}$ can be reconstructed using the previous formula (6) after all path parameters are estimated.

Based on the above discussions, the pseudocode of the proposed NE-DFT algorithm is summarized in Algorithm 2, the proposed algorithm requires the same training sequence length as that of the DFT-CEA, which is $N_{TS} = \lceil N_R^d / N_R^{RF} \rceil \lceil N_T^d / N_T^{RF} \rceil N_T^{RF}$. Moreover, the complexity of calculating the 2D-DFT using the fast Fourier transform (FFT) is $O(N_{DFT} \log_2 N_{DFT})$.

IV. SIMULATION RESULTS

In this section, we evaluate the performance of the proposed NE-DFT algorithm, we consider a typical mmWave massive MIMO system model described in Section II. The ULA at BS and MS are equipped with $N_T = 128$ and $N_R = 64$ antenna elements, respectively. There are $N_T^{RF} = 16$ RF chains at BS and $N_R^{RF} = 8$ RF chains at MS. The spacing between antenna elements is equal to $\lambda/2$, the number of

Algorithm 2 Noise Elimination DFT-Based Algorithm

Input: BS and MS know $N_T, N_R, N_T^{RF}, N_T^{RF}, L, L_d, N_{DFT}, \sigma, \delta_{thres}$ and have $\bar{\mathbf{F}}_{\mathrm{RF}}, \bar{\mathbf{W}}_{\mathrm{RF}}$

Output: Matrix $\mathbf{H} \in \mathbb{C}^{N_R \times N_T}$;

Initialization: $N_T^d = N_T^{RF}, N_R^d = N_R^{RF}$

BS sends $\mathbf{x}_{\mathrm{D}}^{(m)}$ and uses $\mathbf{F}_{\mathrm{RF}}^{(t)}$, MS uses $\mathbf{W}_{\mathrm{RF}}^{(s)}$

calculate $\hat{\hat{\mathbf{H}}}^{(s,t)}$ and stack them $\hat{\hat{\mathbf{H}}}$

calculate $W(k,i)$ and $W_1(k,i) = W(k,i)$

for do $l = 1$ to L_d

  $(\hat{k}_l, \hat{i}_l) = \arg\max_{k,i} |W_l(k,i)|$

  $\rho'_l = W_l(\hat{k}_l, \hat{i}_l)\sqrt{L}/(N_R^d N_T^d)$

  cut out $\tilde{\mathbf{W}}$ from $W_l(k,i)$ and cut out $\tilde{\mathbf{R}}$ from $\rho'_l \left|R(k-k'_l, i-i'_l)\right| / \sqrt{L}$

  $E_l = \left\|\tilde{\mathbf{W}} - \tilde{\mathbf{R}}\right\|^2 / \left\|\tilde{\mathbf{R}}\right\|^2$

  $W_{l+1}(k,i) = W_l(k,i) - \rho'_l R(k-k'_l, i-i'_l)/\sqrt{L}$

end

for do $l = 1$ to L

  if $(1/\sqrt{L})\hat{\rho}_l N_R^d N_T^d > \delta_{thres}$

    $\hat{\rho}_l = \rho'_l, \hat{k}_l = k', \hat{i}_l = i'_l$

    $\hat{\theta}_l^t = \sin^{-1}(-2\hat{i}_l/N_{DFT})$,
    $\hat{\varphi}_l^r = \sin^{-1}(2\hat{k}_l/N_{DFT})$

    $E_l = \inf$

  else

    $(\hat{r}) = \arg\min_r E(r)$

    $\hat{\rho}_l = \rho'_{\hat{r}}, \hat{k}_l = k'_{\hat{r}}, \hat{i}_l = i'_{\hat{r}}$

    $\hat{\theta}_l^t = \sin^{-1}(-2\hat{i}_l/N_{DFT})$,
    $\hat{\varphi}_l^r = \sin^{-1}(2\hat{k}_l/N_{DFT})$

    $E_l = \inf$

  end

end

estimating paths is $L_d = 3L$; the numbers of extracted the rows and columns from submatrix are $N_R^{sub} = 19$ and $N_T^{sub} = 9$, respectively. Since $\mathbf{F}_{\mathrm{RF}}^{(q)}$ switches on only N_T^{RF} antennas, $SNR_d = SNR + 10 * \lg(N_T^{RF}/N_T)$ when all antennas are used. Set the signal power of the training sequence as 1, and the noise variance is $\sigma^2 = 10^{-(SNR+10*\lg(N_T^{RF}/N_T))/10}$. We define NMSE $\mathbb{E}$ as a parameter used to evaluate the performance of channel estimation, and the calculation formula is as follows:

$$\mathbb{E} = \left\|\hat{\mathbf{H}} - \mathbf{H}\right\|^2 / \|\mathbf{H}\|^2, \tag{48}$$

where $\hat{\mathbf{H}}$ denotes the estimated value of the entire channel $\mathbf{H}$.

Fig. 6 compares the NMSE performance between the proposed NE-DFT algorithm and the conventional DFT-CEA. From Fig. 6, we can observe that the curves of the proposed NE-DFT algorithm are below that of DFT-CEA, which indicates that the proposed scheme has significant performance improvement compared to the conventional scheme when $L = 6, 8, 12$. The NMSE difference of the two schemes rises with the SNR increasing. Specifically, for

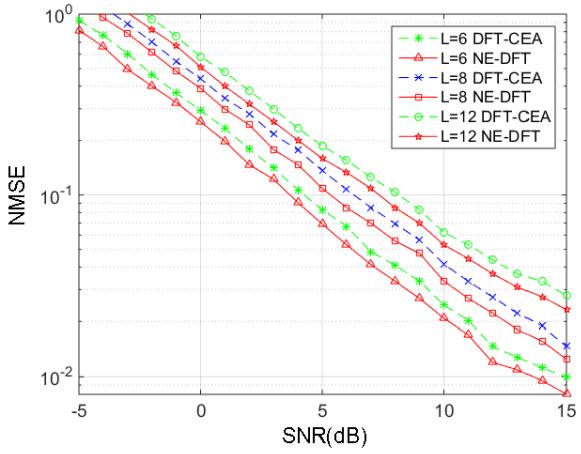

FIGURE 6. NMSE versus SNR for different L with $N_R^d = 39$ and $N_T^d = 78$.

$SNR \in [-5\,dB, 15\,dB]$, the NMSE of the NE-DFT algorithm is less than that of DFT-CEA when $L = 6$. By contrast, our scheme is approximately 1.5 dB away from the conventional scheme at SNR = 15 dB. Moreover, our proposed algorithm is superior to the traditional algorithm by approximately 0.98 dB when SNR = −5 dB. The NMSE performance degrades in low SNR levels under the time-variant channel because the severe noise interference exists in the variant channel, which is consistent with our previous theoretical analysis. Additionally, we compare the NMSE of the two algorithms with $L = 8$; the NMSE of the NE-DFT algorithm is smaller than that of DFT-CEA at approximately 1.3 dB at SNR = 15 dB, and the proposed scheme also achieves approximately 0.91 dB improvement compared with the conventional scheme when SNR = −4 dB. Furthermore, the curve trend of the two algorithms is basically similar when $L = 12$. Our proposed algorithm is superior to the traditional algorithms at approximately 1.3 dB at SNR = 15 dB, and the performance gap between two algorithms reaches 0.9 dB when SNR = −3 dB. It can be seen that the channel estimation accuracy based on the NE-DFT algorithm is better than that of the DFT-CEA, which proves the advantages of our proposed scheme. To summarize, the proposed scheme is superior to the traditional scheme in channel estimation under the time-variant mmWave channel.

Fig. 7 illustrates the NMSE performance against SNR when $L = 8$, N_R^d and N_T^d take different values. The formula for calculating the length of the training sequence is as follows:

$$N_{TS} = \left\lceil N_R^d / N_R^{RF} \right\rceil \left\lceil N_T^d / N_T^{RF} \right\rceil N_T^{RF}, \tag{49}$$

where the length of training sequence varies with N_R^d and N_T^d. We can see that the NMSE decreases with the length N_{TS} increasing, which indicates that the increase of N_{TS} can effectively improve the channel estimation accuracy. The simulation results are basically consistent with the actual scene of mmWave vehicle dynamic communication. Due to

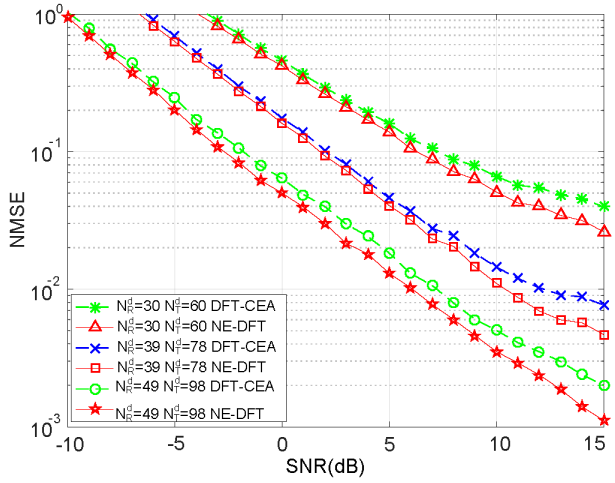

FIGURE 7. NMSE versus SNR for different N_R^d and N_T^d with $L = 8$.

the high mobility of the channel users, the channel estimation accuracy decreases. Therefore, we need to adaptively adjust the training sequence length for time-varying channel estimation. When $N_R^d = 30, N_T^d = 60$ and $SNR \in [-10\,dB, 15\,dB]$, our proposed algorithm is 1.9 dB better than that of the traditional scheme at SNR = 15 dB. Moreover, the NMSE difference between the two schemes decreases with SNR decreasing. Similarly, an approximate 0.45 dB difference between the two schemes can be obtained when SNR $= -3$ dB. In addition, when $N_R^d = 39, N_T^d = 78$ under the same SNR condition, our scheme is approximately 2.2 dB higher than the traditional scheme at SNR = 15 dB, and the gap between the two schemes is approximately 0.5 dB when SNR $= -6$ dB. By contrast, the curve trends when $N_R^d = 39, N_T^d = 78$, $N_R^d = 49, N_T^d = 98$ are similar to that of the curves when $N_R^d = 30, N_T^d = 60$. We can achieve approximately 2.4 dB difference between the two algorithms at SNR = 15 dB, and the gap between the two schemes reaches 0.65 dB when SNR $= -10$ dB. Obviously, the estimation accuracy of our proposed algorithm is significantly improved for different training sequence lengths, and the accuracy of our proposed algorithm increases with the increase of the training sequence. A higher estimation accuracy can be obtained even in the case of the shorter training sequence. Since the mmWave vehicular communications exhibit time-varying channel characteristics, our proposed scheme is more suitable for time-variant mmWave channel estimation in a massive MIMO system.

V. CONCLUSIONS

This paper investigates the channel estimation problem for single-user mmWave massive MIMO in vehicular cellular systems. For the time-varying characteristic of the mmWave communication channel, the NE-DFT scheme with a higher estimation accuracy was proposed. First, several path parameters were estimated by CEA-DFT. Next, a judgment threshold was used to judge the accuracy of each path that has been estimated. Then, the path energy distribution was analyzed and submatrices for energy extraction were designed. Furthermore, the comparison operation was performed between the total channel submatrix and the actual signal submatrix, and the paths with the smallest comparison value in the remaining paths were selected as the real paths, and an auxiliary judgment is developed to estimate enough real paths. Finally, the channel matrix was reconstructed using estimated channel parameters. The performance analysis showed that our proposed algorithm exhibits superior estimation performance under the scene that has a large number of paths, is time-variant and has a shorter training sequence, which effectively reduces noise interference. So our proposed scheme is suitable for the rapidly changing channel in the mmWave band.

REFERENCES

[1] A. Alkhateeb, O. El Ayach, G. Leus, and R. W. Heath, Jr., "Channel estimation and hybrid precoding for millimeter wave cellular systems," *IEEE J. Sel. Topics Signal Process.*, vol. 8, no. 5, pp. 831–846, Oct. 2014.

[2] F. J. Martin-Vega, M. C. Aguayo-Torres, G. Gomez, J. T. Entrambasaguas, and T. Q. Duong, "Key technologies, modeling approaches, and challenges for millimeter-wave vehicular communications," *IEEE Commun. Mag.*, vol. 56, no. 10, pp. 28–35, Oct. 2018.

[3] J. G. Andrews, S. Buzzi, W. Choi, S. V. Hanly, A. Lozano, A. C. K. Soong, and J. C. Zhang, "What will 5G be?" *IEEE J. Sel. Areas Commun.*, vol. 32, no. 6, pp. 1065–1081, Jun. 2014.

[4] O. E. Ayach, S. Rajagopal, S. Abu-Surra, Z. Pi, and R. W. Heath, Jr., "Spatially sparse precoding in millimeter wave MIMO systems," *IEEE Trans. Wireless Commun.*, vol. 13, no. 3, pp. 1499–1513, Mar. 2014.

[5] K. Venugopal, A. Alkhateeb, N. G. Prelcic, and R. W. Heath, Jr., "Channel estimation for hybrid architecture-based wideband millimeter wave systems," *IEEE J. Sel. Areas Commun.*, vol. 35, no. 9, pp. 1996–2009, Sep. 2017.

[6] W. Shen, L. Dai, J. An, P. Fan, and R. W. Heath, Jr., "Channel estimation for orthogonal time frequency space (OTFS) massive MIMO," 2019, *arXiv:1903.0944*. [Online]. Available: https://arxiv.org/abs/1903.09441

[7] S. H. Lim, J. Bae, S. Kim, B. Shim, and J. Won Choi, "Efficient beam training and channel estimation for millimeter wave communications under mobility," 2018, *arXiv:1804.07973*. [Online]. Available: http://arxiv.org/abs/1804.07973

[8] C. Zhang, W. Zhang, W. Wang, L. Yang, and W. Zhang, "Research challenges and opportunities of UAV millimeter-wave communications," *IEEE Wireless Commun.*, vol. 26, no. 1, pp. 58–62, Feb. 2019.

[9] N. Garcia, H. Wymeersch, E. G. Strom, and D. Slock, "Location-aided mm-wave channel estimation for vehicular communication," in *Proc. IEEE 17th Int. Workshop Signal Process. Adv. Wireless Commun. (SPAWC)*, Jul. 2016, pp. 1–5.

[10] X. Gao, L. Dai, S. Han, C.-L. I, and X. Wang, "Reliable beamspace channel estimation for millimeter-wave massive MIMO systems with lens antenna array," *IEEE Trans. Wireless Commun.*, vol. 16, no. 9, pp. 6010–6021, Sep. 2017.

[11] L. Kong, M. K. Khan, F. Wu, G. Chen, and P. Zeng, "Millimeter-wave wireless communications for IoT-cloud supported autonomous vehicles: Overview, design, and challenges," *IEEE Commun. Mag.*, vol. 55, no. 1, pp. 62–68, Jan. 2017.

[12] J. Choi, V. Va, N. Gonzalez-Prelcic, R. Daniels, C. R. Bhat, and R. W. Heath, Jr., "Millimeter-wave vehicular communication to support massive automotive sensing," *IEEE Commun. Mag.*, vol. 54, no. 12, pp. 160–167, Dec. 2016.

[13] M. M. Awad, K. G. Seddik, and A. Elezabi, "Channel estimation and tracking algorithms for harsh vehicle to vehicle environments," in *Proc. IEEE 82nd Veh. Technol. Conf. (VTC-Fall)*, Sep. 2015, pp. 6–9.

[14] Z. Sha, Z. Wang, and S. Chen, "Harmonic retrieval based baseband channel estimation for millimeter wave OFDM systems," *IEEE Trans. Veh. Technol.*, vol. 68, no. 3, pp. 2668–2681, Mar. 2019.

[15] *5G Automotive Vision, 5G-PPP*, Eur. Commission, Brussels, Belgium, 2015.

[16] T. S. Rappaport, S. Sun, R. Mayzus, H. Zhao, Y. Azar, K. Wang, G. N. Wong, J. K. Schulz, M. Samimi, and F. Gutierrez, "Millimeter wave mobile communications for 5G cellular: It will work!" *IEEE Access*, vol. 1, pp. 335–349, May 2013.

[17] X. Wu, W.-P. Zhu, M. Lin, and J. Yan, "Joint Doppler and channel estimation with nested arrays for millimeter wave communications," in *Proc. IEEE Global Commun. Conf. (GLOBECOM)*, Dec. 2018, pp. 1–6.
[18] X. Gao, L. Dai, S. Han, I. Chih-Lin, and F. Adachi, "Beamspace channel estimation for 3D lens-based millimeter-wave massive MIMO systems," in *Proc. 8th Int. Conf. Wireless Commun. Signal Process. (WCSP)*, Oct. 2016, pp. 1–5.
[19] X. Gao, L. Dai, Y. Zhang, T. Xie, X. Dai, and Z. Wang, "Fast channel tracking for terahertz beamspace massive MIMO systems," *IEEE Trans. Veh. Technol.*, vol. 66, no. 7, pp. 5689–5696, Jul. 2017.
[20] S. Montagner, N. Benvenuto, and P. Baracca, "Channel estimation using a 2D DFT for millimeter-wave systems," in *Proc. IEEE 81st Veh. Technol. Conf. (VTC Spring)*, May 2015, pp. 1–5.
[21] W. Lu, W. Zou, and X. Liu, "An adaptive channel estimation algorithm for millimeter wave cellular systems," *J. Commun. Inf. Netw.*, vol. 1, no. 2, pp. 37–44, Aug. 2016.
[22] S. Shaham, M. Ding, M. Kokshoorn, Z. Lin, S. Dang, and R. Abbas, "Fast channel estimation and beam tracking for millimeter wave vehicular communications," 2018, *arXiv:1806.0016*. [Online]. Available: https://arxiv.org/abs/1806.00161
[23] X. Ma, F. Yang, S. Liu, J. Song, and Z. Han, "Sparse channel estimation for MIMO-OFDM systems in high-mobility situations," *IEEE Trans. Veh. Technol.*, vol. 67, no. 7, pp. 6113–6124, Jul. 2018.
[24] X. Sun, C. Qi, and G. Y. Li, "Beam training and allocation for multiuser millimeter wave massive MIMO systems," *IEEE Trans. Wireless Commun.*, vol. 18, no. 2, pp. 1041–1053, Feb. 2019.
[25] W. Ma and C. Qi, "Channel estimation for 3-D lens millimeter wave massive MIMO system," *IEEE Commun. Lett.*, vol. 21, no. 9, pp. 2045–2048, Sep. 2017.
[26] D. Fan, F. Gao, G. Wang, Z. Zhong, and A. Nallanathan, "Angle domain signal processing-aided channel estimation for indoor 60-GHz TDD/FDD massive MIMO systems," *IEEE J. Sel. Areas Commun.*, vol. 35, no. 9, pp. 1948–1961, Sep. 2017.

ZHAO YI (Student Member, IEEE) received the M.S. degree in communication and information systems from the Guilin University of Electronic Technology, Guilin, China, in 2013. He is currently pursuing the Ph.D. degree with the School of Information and Communication Engineering, Beijing University of Posts Telecommunications (BUPT), Beijing, China. From 2013 to 2017, he was a Lecturer with the Guilin University of Aerospace Technology. His current research interests include millimeter wave wireless communication and massive MIMO techniques.

WEIXIA ZOU (Member, IEEE) received the bachelor's degree from Tongji University, in 1994, the master's degree from Shandong University, in 2002, and the Ph.D. degree from the Beijing University of Posts Telecommunications (BUPT), China, in 2006. She is currently an Associate Professor with BUPT. Her current research interests include new technologies of short-range wireless communications and the electromagnetic compatibility.